



**Fermi National Accelerator Laboratory**

**FERMILAB-Conf-97/233-E**

**DØ**

**Physics of the Top Quark at DØ**  
**New Measurement of the Production Cross Section and Mass**

Krzysztof Genser  
For the DØ Collaboration

*Fermi National Accelerator Laboratory  
P.O. Box 500, Batavia, Illinois 60510*

July 1997

*Presented at the 1997 Les Rencontres de Physique de la Vallee d'Aoste, Results and Perspectives in Particle Physics, La Thuile, Aosta Valley, Italy, March 2-8, 1997*

## **Disclaimer**

*This report was prepared as an account of work sponsored by an agency of the United States Government. Neither the United States Government nor any agency thereof, nor any of their employees, makes any warranty, expressed or implied, or assumes any legal liability or responsibility for the accuracy, completeness, or usefulness of any information, apparatus, product, or process disclosed, or represents that its use would not infringe privately owned rights. Reference herein to any specific commercial product, process, or service by trade name, trademark, manufacturer, or otherwise, does not necessarily constitute or imply its endorsement, recommendation, or favoring by the United States Government or any agency thereof. The views and opinions of authors expressed herein do not necessarily state or reflect those of the United States Government or any agency thereof.*

## **Distribution**

*Approved for public release; further dissemination unlimited.*

# Physics of the Top Quark at DØ New Measurement of the Production Cross Section and Mass <sup>1</sup>

Krzysztof Genser

*Fermilab*  
*Batavia, IL 60510-0500, USA*

for DØ Collaboration

## Abstract

We present a measurement of the  $t\bar{t}$  production cross section in  $p\bar{p}$  collisions at  $\sqrt{s} = 1.8$  TeV and a measurement of top quark mass  $m_t$  by the DØ experiment at the Fermilab Tevatron. The measurements are based on the data from the 1992–1996 run during which the DØ detector was exposed to the integrated luminosity of approximately  $125 \text{ pb}^{-1}$ . We observe 39  $t\bar{t}$  candidate events in the dilepton and lepton+jets decay channels with an expected background of  $13.7 \pm 2.2$  events. We measure the top quark mass  $m_t$  using a two constraint fit to  $m_t$  in  $t\bar{t} \rightarrow bW^+ \bar{b}W^-$  final states with one  $W$  decaying to  $q\bar{q}$  and the other to  $e\nu$  or  $\mu\nu$ . Events are binned in the fit mass versus a measure of probability for events to be the signal rather than a background. Likelihood fits to the data yield  $m_t = 173.3 \pm 5.6$  (stat)  $\pm 6.2$  (syst) GeV/c<sup>2</sup>. For this mass we measure the  $t\bar{t}$  production cross section to be  $5.5 \pm 1.8$  pb.

---

<sup>1</sup>presented at the 1997 Les Rencontres de Physique de la Vallée d'Aoste, Results and Perspectives in Particle Physics, La Thuile, Aosta Valley, Italy, March 2–8, 1997

# 1 Introduction

Since the discovery of the top quark in 1995 at the Fermilab Tevatron [1, 2] a lot of effort was put into precise measurements of its production cross section and mass in order to test the predictions of the Standard Model (SM).

According to the SM, in  $p\bar{p}$  collisions at  $\sqrt{s} = 1.8$  TeV, the top (and anti-top) quarks with  $m_t \approx 180$  GeV/ $c^2$  are predominantly pair produced through  $q\bar{q}$  annihilation ( $\approx 90\%$ ) or gluon fusion ( $\approx 10\%$ ). Due to their large mass, the top quarks decay before they hadronize; nearly all ( $\geq 99.8\%$ ) decay to a  $W$  boson and a  $b$  quark. The subsequent  $W$  decay determines the signatures of  $t\bar{t}$  decay. We have studied the dilepton channels in which both  $W$  bosons decay either to  $e\nu$  or  $\mu\nu$  and the lepton+jets channel in which one  $W$  boson decays to  $e\nu$  or  $\mu\nu$  and the other  $W$  decays hadronically.

In this paper we present measurements of the  $t\bar{t}$  production cross section ( $\sigma_{t\bar{t}}$ ) using the dilepton and lepton+jets channels[3] and the top quark mass using the lepton+jets channel[4]. We have used our entire data sample of up to  $(125 \pm 7 \text{ pb}^{-1})$  per channel collected during the 1992–1996 Tevatron Collider run. A detailed description of the DØ detector, trigger, and algorithms for reconstructing jets and missing transverse energy  $\cancel{E}_T$  can be found in Refs. [5, 6]. The current electron and muon identification algorithms were further improved to provide better rejection of backgrounds and increased efficiencies than those used in Ref. [6].

## 2 Measurement of Top Quark Production Cross Section

### 2.1 Dilepton Channels

The dilepton channels include  $ee$ ,  $e\mu$  and  $\mu\mu$  channels. The signature consists of two isolated high  $p_T$  leptons, two or more jets, and large  $\cancel{E}_T$ . The selection criteria are summarized in Table 1. The number of observed events in the data are shown in Table 2 together with the expected number of background and signal events. The dominant sources of background for the dilepton channels are  $Z$  boson, Drell-Yan, and vector boson pair production together with jets faking leptons. Fig. 1 shows the  $H_T$  distribution for the dilepton channels for the data, expected top signal and background. One can see the effectiveness of the  $H_T$  cut. There are three  $e\mu$  events, one  $ee$  event, and one  $\mu\mu$  event

that survive the selection criteria.

## 2.2 $e\nu$ Channel

The  $e\nu$  channel is an inclusive channel whose signature consists of an isolated high  $p_T$  electron, large  $\cancel{E}_T$  and two or more jets.

This channel accepts top signal mainly from dilepton events containing an electron and not seen in the  $e\mu$  and  $ee$  channels. Those can be  $e\tau$  events or genuine  $e\mu$  and  $ee$  events which have  $p_T$  of one of the leptons too low to pass the lepton  $p_T$  cut but  $p_T$  of the neutrino high enough to pass the  $M_T^{e\nu}$  cut described below. Another category of events entering this channel is  $e\mu$  and  $ee$  events with the  $\mu$  or  $e$  lost due to lepton identification

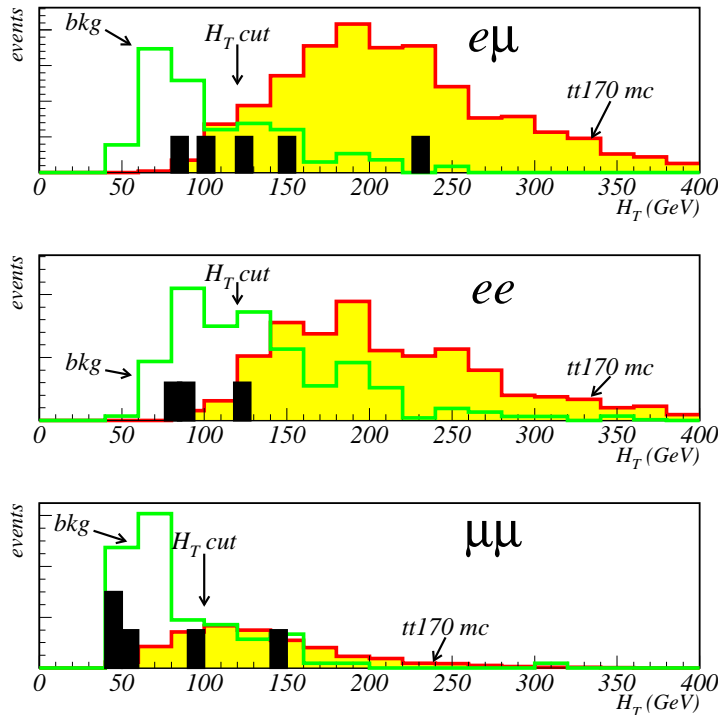


Figure 1:  $H_T$  distribution for dilepton channels. Black rectangles represent the data events, histograms show expected top and sum of the background distributions. The arrows show the placement of the  $H_T$  cut. All cuts except  $H_T$  cut as shown are applied.

inefficiencies. This channel also contains some admixture of the  $e$ +jets top decays which fail the standard selection cuts. The selection criteria are summarized in Table 1. The two dominant sources of background for this channel are  $W$  + jets and QCD multijet events. The cut on the  $e\nu$  transverse mass  $M_T^{e\nu}$  suppresses the  $W$  + jets background. The cut on  $\Delta\phi(\cancel{E}_T, E_T^{2ndjet(e)})$  which is the separation in the azimuthal angle between the  $\cancel{E}_T$  vector and the second highest  $E_T$  jet, where an electron is also counted as a jet, together with  $\cancel{E}_T$  cut is used to suppress QCD multijet events. The event yields are shown in Table 2. Fig. 2 shows the  $\cancel{E}_T$  versus  $M_T^{e\nu}$  distributions for data, the expected top signal and the background. The four data events passing all the cuts lay well within the signal region defined by the solid lines shown.

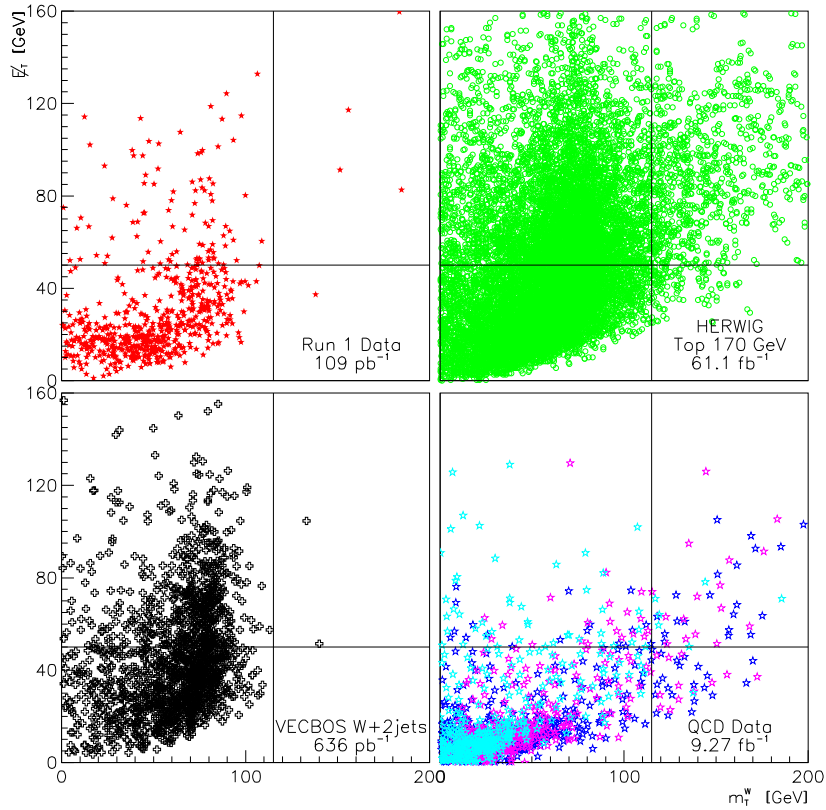


Figure 2: Event  $\cancel{E}_T$  versus  $e\nu$  transverse mass  $M_T^{e\nu}$  for data signal sample, expected top, expected  $W$  + 2jets and QCD three jet data sample with one of the jets faking an electron. All cuts are applied except of  $\cancel{E}_T$  and  $M_T^{e\nu}$  which are shown using the full lines.

### 2.3 Lepton+jets Channels

The lepton+jets channels include  $\ell$ +jets (*topological*) and  $\ell$ +jets/ $\mu$  (*b-tag*) channels.

The signature of the  $\ell$ +jets (*topological*) channel consists of one isolated high  $p_T$  lepton,  $\cancel{E}_T$  and four jets. The selection criteria are summarized in Table 1. The number of observed events in the data are shown in Table 2 together with the expected number of background and signal events. The dominant sources of background for this channel are  $W$  + jets and QCD multijet events. These backgrounds are suppressed by cutting on the  $H_T$ , the aplanarity  $\mathcal{A}$  (computed using  $W$  boson and jet momenta in the laboratory frame[8]),  $E_T^L$  (the scalar sum of the lepton  $E_T$ ) and  $\cancel{E}_T$ . The optimal variables and their threshold values were determined using a random grid search technique[7] to maximize the expected precision of the  $t\bar{t}$  cross section measurement. Fig. 3 shows the  $\mathcal{A}$  versus

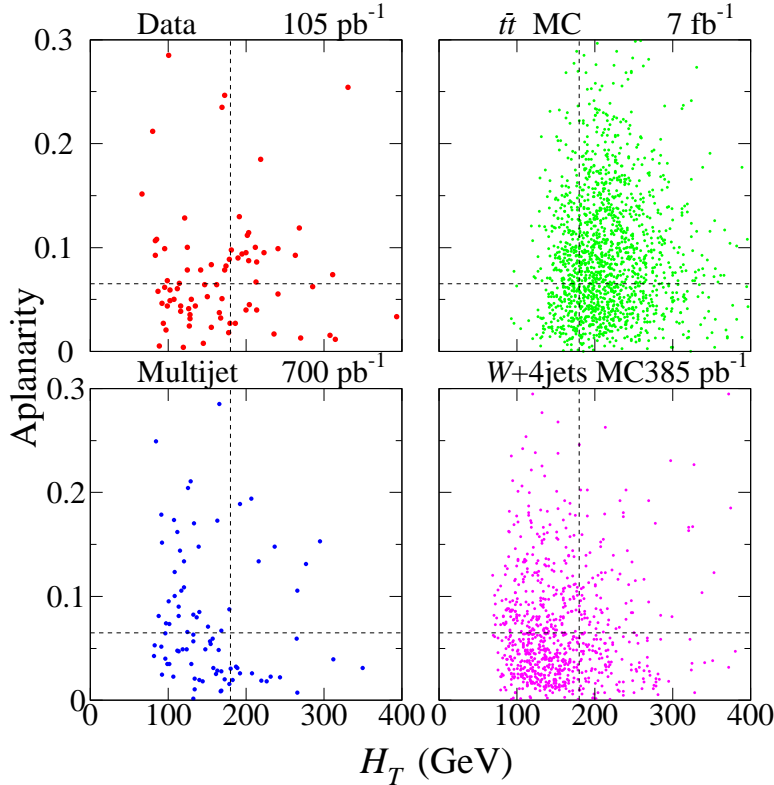


Figure 3: Distributions of  $\mathcal{A}$  versus  $H_T$  for  $\ell$ +jets data events compared to expectations for higher luminosity samples of  $t\bar{t}$  ( $m_t = 170 \text{ GeV}/c^2$ ), multijet, and  $W$ +4jets backgrounds. The dashed lines represent the threshold values used for the selection.

$H_T$  distribution for  $\ell$ +jets (*topological*) data sample, signal MC, QCD multijet and  $W$ +4 jets events. The cuts indicated by the dashed lines provide a good separation between the expected signal and backgrounds.

The signature of the  $\ell$ +jets/ $\mu$  (*b-tag*) channel consists of one isolated high  $p_T$  lepton,  $\cancel{E}_T$  and three jets one of which has to have a tag muon associated with it. The tag muon is defined as separated by no more than 0.5 in the  $\Delta\mathcal{R}_{\text{jet}} = \sqrt{\Delta\eta^2 + \Delta\phi^2}$  space from the jet and having  $p_T^\mu > 4$ . Only  $\approx 2\%$  of background events as compared to  $\approx 20\%$  of  $t\bar{t}$  events have a tag muon. The selection criteria for this channel are summarized in Table 1 and the event yields are shown in Table 2.  $W$  + jets and QCD multijet production are the dominant sources of background and are suppressed by the b-tag requirement and cuts on  $\mathcal{A}$  and  $H_T$ . Fig. 4 shows the jet multiplicity spectrum of  $\ell$ +jets/ $\mu$  events and the background estimates before event shape ( $\mathcal{A}, H_T$ ) cuts. There is good agreement for one and two jet samples, while the excess of data events at three or more jets indicates  $t\bar{t}$  production.

The lepton+jets selection criteria yield 9  $e$ +jets, 10  $\mu$ +jets, 5  $e$ +jets/ $\mu$ , and 6  $\mu$ +jets/ $\mu$  events.

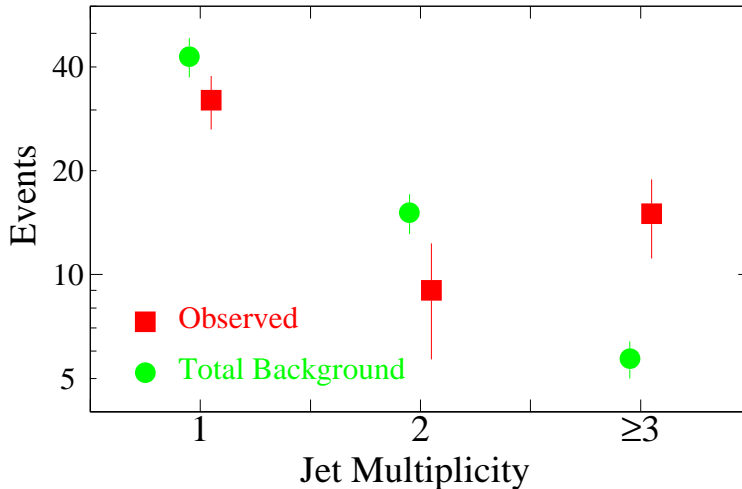


Figure 4: Jet multiplicity spectrum of  $\ell$ +jets/ $\mu$  events before imposing event shape ( $\mathcal{A}, H_T$ ) criteria, compared to background estimates.

Table 1: Kinematic selection criteria for decay channels included in the cross section measurement. An event may populate only one channel. All energies are in GeV.  $\eta$  is the pseudorapidity;  $H_T$  for  $\ell$ +jets channels is the scalar sum of the  $E_T$  of all jets with  $E_T \geq 15$  GeV, for the dilepton channels  $H_T$  also includes the  $E_T$  of the leading electron;  $\mathcal{A}$  is the aplanarity;  $E_T^{2ndjet(e\ell)}$  in  $\Delta\phi(\cancel{E}_T, E_T^{2ndjet(e\ell)})$  for the  $e\nu$  channel is the  $E_T$  of the second highest  $E_T$  jet, where an electron is also counted as a jet. Jets were reconstructed with cones of half-angle  $\Delta\mathcal{R} \equiv \sqrt{\Delta\phi^2 + \Delta\eta^2} = 0.5$

	dilepton			$e\nu$	$\ell$ +jets <i>topological</i>	$\ell$ +jets/ $\mu$ <i>b-tag</i>
	$ee$	$e\mu$	$\mu\mu$			
lepton $p_T$	$> 20$	$> 15$	$> 15$	$> 20$	$> 20$	$> 20$
electron $ \eta $	$< 2.5$	$< 2.5$	—	$< 1.1$	$< 2.0$	$< 2.0$
muon $ \eta $	—	$< 1.7$	$< 1.7$	—	$< 1.7$	$< 1.7$
$\cancel{E}_T$	$> 25$	$> 20$	—	$> 50$	$> 25$ ( $e$ ) $> 20$ ( $\mu$ )	$> 20$
jet $E_T$	$> 20$	$> 20$	$> 20$	$> 30$	$> 15$	$> 20$
jet $ \eta $	$< 2.5$	$< 2.5$	$< 2.5$	$< 2.0$	$< 2.0$	$< 2.0$
# of jets	$\geq 2$	$\geq 2$	$\geq 2$	$\geq 2$	$\geq 4$	$\geq 3$
$H_T$	$> 120$	$> 120$	$> 100$	—	$> 180$	$> 110$
$\mathcal{A}$	—	—	—	—	$> 0.065$	$> 0.040$
$E_T^L$	—	—	—	—	$> 60$	—
$\eta_W$	—	—	—	—	$< 2.0$	—
tag muon	—	—	—	—	veto	$p_T > 4$ $\Delta\mathcal{R}_{jet} < 0.5$
Prob( $\chi^2(Z \rightarrow \mu\mu)$ )	—	—	$< 0.01$	—	—	$< 0.01$ ( $\mu$ )
$M_T^{e\nu}$	—	—	—	$> 115$	—	—
$\Delta\phi(\cancel{E}_T, E_T^{2ndjet(e\ell)})$	—	—	—	$> 0.5$	—	—

## 2.4 Systematic Errors; $t\bar{t}$ Signal and Background Predictions

The  $t\bar{t}$  production was simulated using the HERWIG event generator[9] and a GEANT model of the DØ detector[10] for top quark masses between 100 and 250 GeV/ $c^2$ . The expected number of signal events shown in Table 2 are computed using the cross section of Ref. [11]. The numbers include the events resulting from  $W \rightarrow \tau\nu$  decays that pass the selection

Table 2: Number of events seen in the data and expected number of background and signal events.  $t\bar{t}$  production cross section from [11].

event	dilepton			$e\nu$	$\ell$ +jets	$\ell$ +jets/ $\mu$	total
	$ee$	$e\mu$	$\mu\mu$		<i>topolo-</i> <i>gical</i>	<i>b-tag</i>	
yields							
data	1	3	1	4	19	11	39
background	$0.5\pm 0.1$	$0.2\pm 0.2$	$0.7\pm 0.2$	$1.2\pm 0.4$	$8.7\pm 1.7$	$2.4\pm 0.5$	$13.7\pm 2.2$
signal							
$m_t$ [GeV/ $c^2$ ]							
150	$1.9\pm 0.3$	$3.2\pm 0.7$	$0.8\pm 0.1$	$2.5\pm 0.8$	$18.3\pm 6.3$	$9.1\pm 1.7$	$35.9\pm 8.8$
170	$1.2\pm 0.2$	$2.2\pm 0.5$	$0.6\pm 0.1$	$1.7\pm 0.5$	$14.1\pm 3.1$	$5.8\pm 1.0$	$25.7\pm 4.6$
190	$0.8\pm 0.1$	$1.4\pm 0.3$	$0.4\pm 0.1$	$1.1\pm 0.3$	$9.2\pm 1.4$	$3.7\pm 0.6$	$16.6\pm 2.4$

cuts.

We divide the backgrounds into the physics backgrounds, which have similar final states as the signal process, and instrumental backgrounds in which objects in the final state were misidentified. The physics backgrounds are estimated using MC. Specifically, the distributions of the  $W$ +jets background are modeled using the VECBOS event generator[13] which is interfaced to HERWIG MC to fragment the partons. The normalization of this background is derived from the data. Instrumental backgrounds for all channels are estimated from the data, using control samples consisting of multijet events and the measured probability for misidentifying a jet as a lepton[6]. The background estimates are summarized in Table 2. The errors quoted in Table 2 include the uncertainty in the jet energy scale, the uncertainty of the theoretical cross sections, differences between the HERWIG and ISAJET[12] event generators, lepton identification, and trigger efficiencies.

## 2.5 Summary of the Cross Section measurement

Thirty nine events satisfy the selection criteria. We expect  $13.7\pm 2.2$  events from background sources and  $24.2\pm 4.1$   $t\bar{t}$  events, assuming  $m_t = 173$  GeV/ $c^2$  and the predicted cross section of Ref. [11]. Fig. 5 shows the measured  $t\bar{t}$  cross section versus top quark mass, compared to three theory calculations[11, 14, 15]. The error band accounts for

statistical and systematic uncertainties, both in the backgrounds and signal acceptances, and takes into account the correlations among all the channels. Our measurement is in a very good agreement with the theoretical predictions.

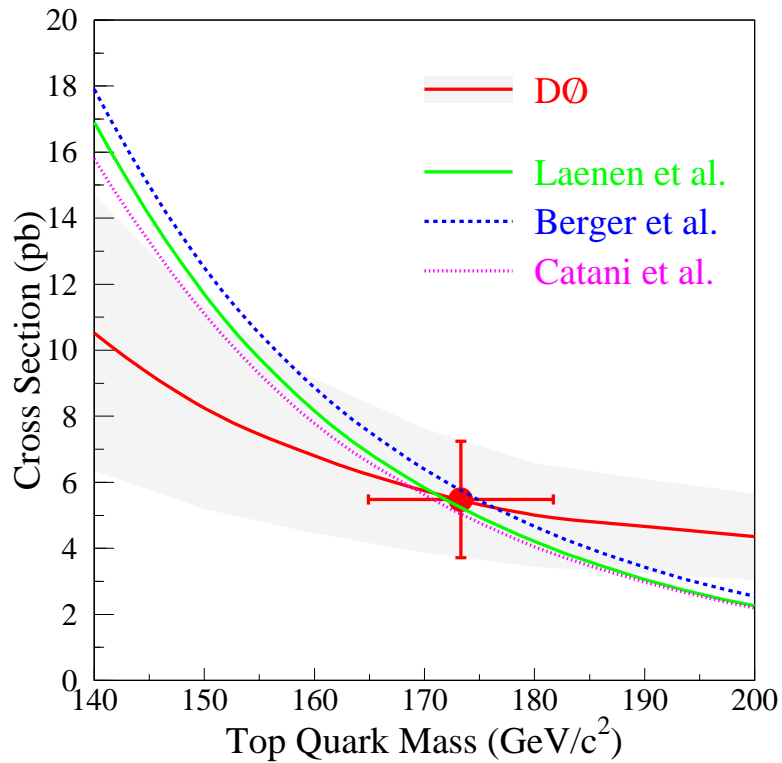


Figure 5: Measured  $t\bar{t}$  production cross section as a function of  $m_t$  (shaded band). The point with error bars is the cross section for the measured top quark mass at D0. Three different theoretical estimates are also shown.

## 3 Measurement of Top Quark Mass in Lepton+Jets Channel

### 3.1 Initial Event Selection

The criteria used to select events used in the mass measurement are similar to the ones used for the  $\ell$ +jets (*topological*) sample described above (cf. Table 1) with the difference that neither  $H_T$ , nor the aplanarity  $\mathcal{A}$  cuts are applied and no *b-tag* veto was required. The  $H_T$  cut is avoided as it is strongly correlated with the  $m_t$ ; 90 events pass those initial cuts.

### 3.2 Two constraint (2C) kinematic Fit

Once this initial selection is done, for each event passing the above cuts, we make a two constraint (2C) kinematic fit [16] to the  $t\bar{t} \rightarrow (\ell\nu b)(q\bar{q}\bar{b})$  hypothesis which yields a  $\chi^2$  and  $m_{\text{fit}}$ . Both reconstructed  $W$  masses are constrained to equal the  $W$  pole mass, and the same fit mass  $m_{\text{fit}}$  is assigned to both the  $t$  and  $\bar{t}$  quarks. If the event contains more than four accepted jets, only the four jets with highest  $E_T$  are used. In  $\approx 50\%$  of MC top events, these jets correspond to the  $b$ ,  $\bar{b}$ ,  $q$ , and  $\bar{q}$ . With (without) a  $\mu$  tag in the event, there are 6 (12) possible fit assignments of these jets to the quarks, each having two solutions to the  $\nu$  longitudinal momentum  $p_z^\nu$ . We use  $m_{\text{fit}}$  only from the permutation with lowest  $\chi^2$ , which is the correct choice for  $\approx 20\%$  of MC top events. We require that  $\chi^2 < 10.0$  which leaves us with 77 events out of which 5 events have a b-tag.

### 3.3 Multivariate Discriminants

Next step is to assign a probability for an event to originate from  $t\bar{t}$  production. We do it using four variables which are chosen to minimize their correlation with  $m_t$ . The variables are:  $x_1 \equiv \cancel{E}_T$ ;  $x_2 \equiv \mathcal{A}$ , the aplanarity;  $x_3 \equiv H_{T2}/H_z$  which measures the event's centrality, where  $H_z$  is the sum of  $|p_z|$  of lepton,  $\nu$ , and the jets, and  $H_{T2}$  is the sum of all jet  $|E_T|$  except the highest;  $x_4 \equiv \Delta\mathcal{R}_{jj}^{\text{min}} E_T^{\text{min}}/E_T^L$  measures the extent to which jets are clustered together, where  $\Delta\mathcal{R}_{jj}^{\text{min}}$  is the minimum  $\Delta\mathcal{R}$  of the six pairs of four jets, and  $E_T^{\text{min}}$  is the smaller jet  $E_T$  from the minimum  $\Delta\mathcal{R}$  pair. As shown for the background dominated  $W+3$  jets sample in Fig. 6(c-f),  $x_1$ - $x_4$  are reasonably well modeled by MC. The four variables are combined to form a multivariate discriminant. We use two methods to form such a

discriminant. In our “low bias” (LB) method, we first parameterize  $\mathcal{L}_i(x_i) \equiv s_i(x_i)/b_i(x_i)$ ,

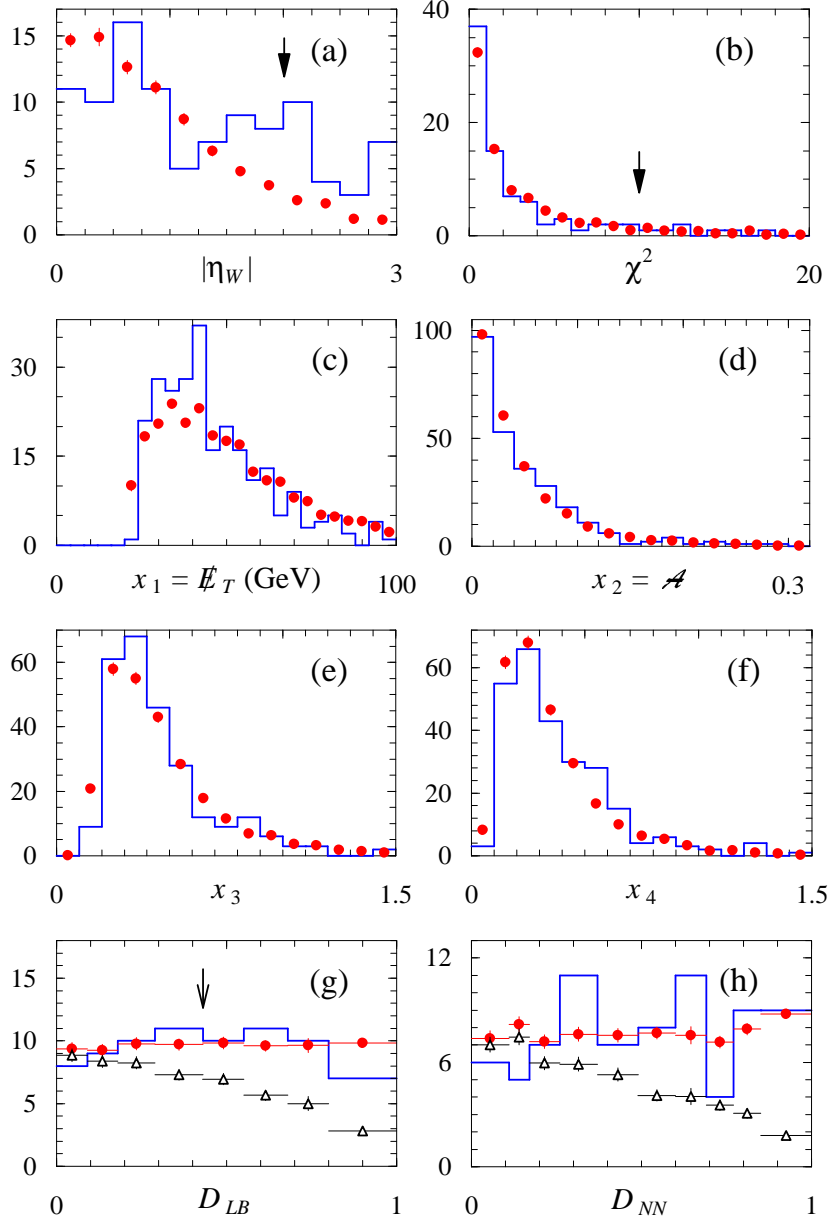


Figure 6: Events per bin versus event selection variables defined in the text, plotted for (a–b, g–h) top quark mass analysis samples, and (c–f)  $W+3$  jets control samples. Histograms are data, filled circles are expected top + background mixture, and open triangles are expected background only. Solid arrows in (a–b) show cuts applied to all events; the open arrow in (g) illustrates the LB cut. The nonuniform bin widths in (g–h) are chosen to yield uniform bin populations.

where  $s_i$  and  $b_i$  are the top signal and background densities in each variable, integrating over the others. We form the log likelihood  $\ln \mathcal{L} \equiv \sum_i \omega_i \ln \mathcal{L}_i$ , where the weights  $\omega_i$  are adjusted slightly away from unity to nullify the average correlation (“bias”) of  $\mathcal{L}$  with  $m_{\text{fit}}$ , and for each event we set  $D_{\text{LB}} = \mathcal{L}/(1 + \mathcal{L})$ . In our neural network (NN) method, we use a three layer feed-forward NN with four input nodes fed by  $\mathbf{x}$ , five hidden nodes, and one output node, trained on samples of top signal (background) with density  $s(\mathbf{x})$  ( $b(\mathbf{x})$ ) [17]. For a given event, the network output  $D_{\text{NN}}$  approximates the ratio  $s(\mathbf{x})/(s(\mathbf{x}) + b(\mathbf{x}))$ . Fig.7 shows the signal and background sample separation using both discriminants. In both cases one can clearly identify the signal and background enriched regions.

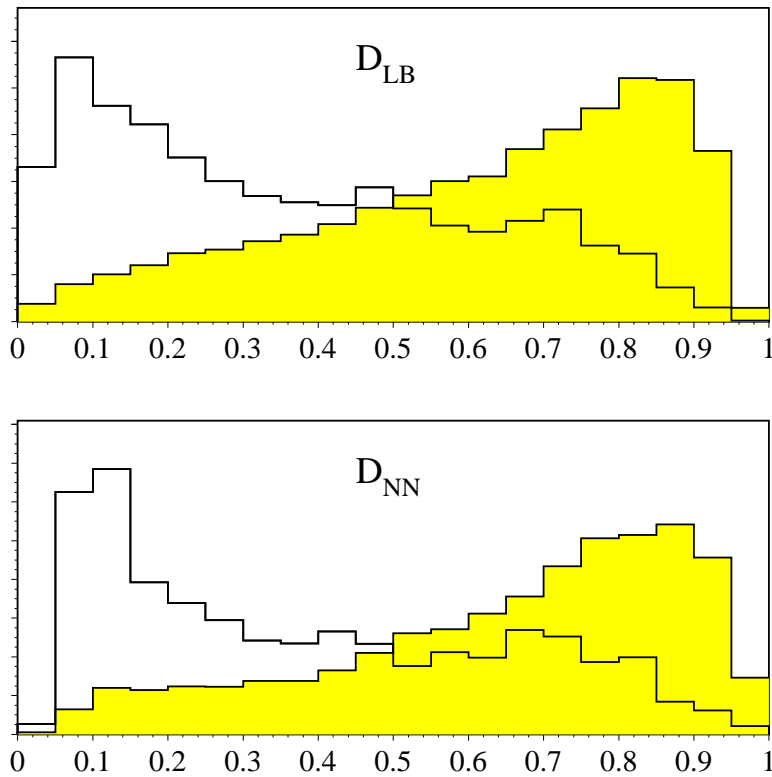


Figure 7: Events per bin versus  $D_{\text{LB}}$  and  $D_{\text{NN}}$  discriminants. The unshaded histograms represent the sum of the backgrounds, the shaded ones show the  $t\bar{t}$  MC for  $m_t = 175$  GeV/ $c^2$

### 3.4 Likelihood $m_t$ Fit

Once the discriminants are defined, we bin events in a two-dimensional array with abscissa  $m_{\text{fit}}$  and ordinate  $D(\mathbf{x})$ . We divide the abscissa into 20 equipopulated  $m_{\text{fit}}$  bins. In the LB case we divide the ordinate into signal and background dominated bins according to whether the LB cut is or is not passed. This cut is satisfied if  $D_{\text{LB}} > 0.43$  and  $H_{T2} > 90$  GeV or if a b-tag exists. In the NN case we divide the ordinate into ten bins in  $D_{\text{NN}}$ , independent of  $H_{T2}$  or b-tagging. Fig. 6(g-h) shows that  $D_{\text{LB}}$  and  $D_{\text{NN}}$  are distributed as predicted and provide comparable discrimination. Fig. 8 exhibits the arrays for the NN method. Little correlation between  $D_{\text{NN}}$  and  $m_{\text{fit}}$  is evident in the expected signal or background distributions. One can clearly identify the background and signal

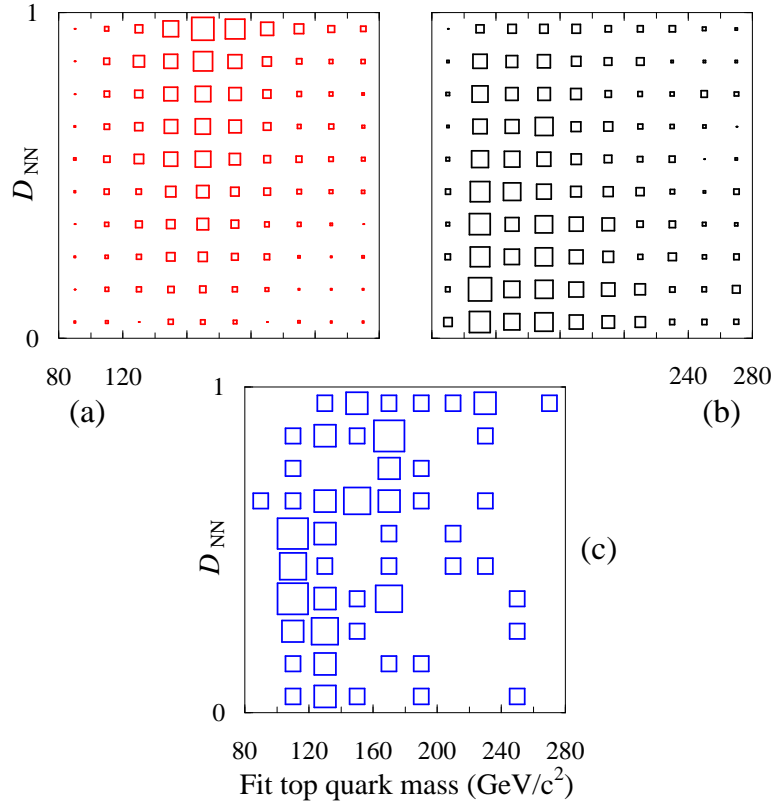


Figure 8: Events per bin ( $\propto$  areas of boxes) versus  $D_{\text{NN}}$  (ordinate) and  $m_{\text{fit}}$  (abscissa) for (a) expected 172  $\text{GeV}/c^2$  top signal, (b) expected background, and (c) data.  $D_{\text{NN}}$  is binned as in Fig. 6(h).

contributions in the data. Fig. 9 shows the distributions of  $m_{\text{fit}}$  for data (a) passing and (b) failing the LB cut.

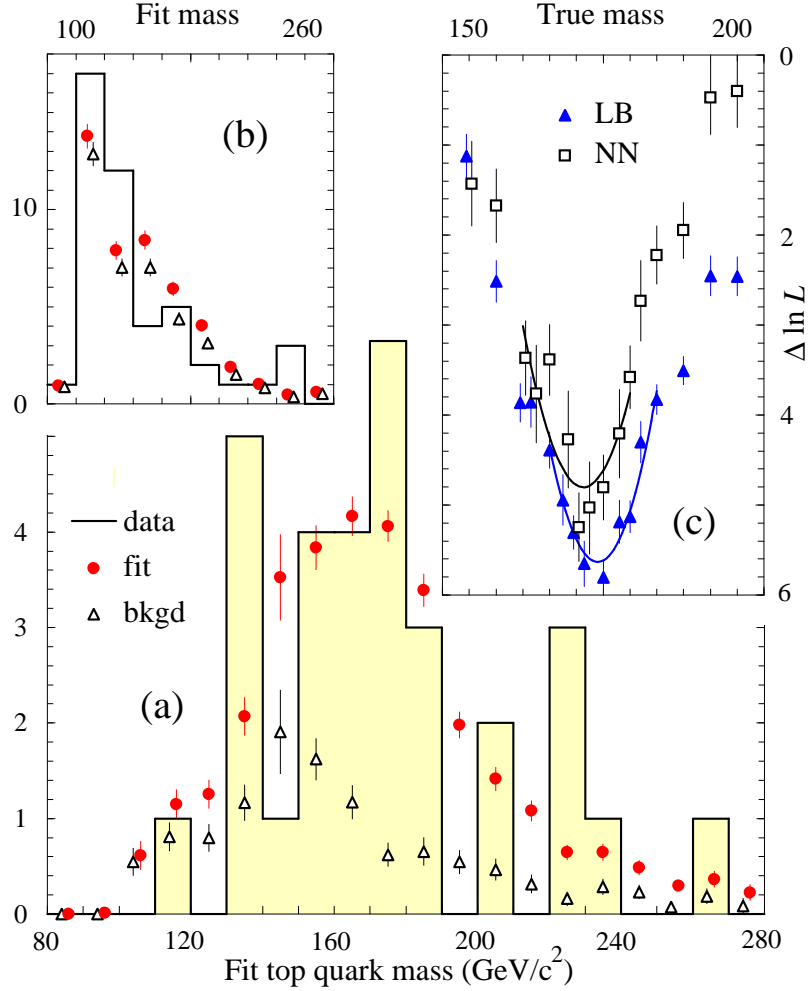


Figure 9: (a–b) Events per bin versus  $m_{\text{fit}}$  for events (a) passing or (b) failing the LB cut. Histograms are data, filled circles are the predicted mixture of top and background, and open triangles are predicted background only. The circles and triangles are the average of the LB and NN fit predictions, which differ by  $<10\%$ . (c) Log of arbitrarily normalized likelihood  $L$  versus true top quark mass  $m_t$  for the LB (filled triangles) and NN (open squares) fits, with errors due to finite top MC statistics. The curves are quadratic fits to the lowest point and its 8 nearest neighbors. In MC studies, 7% (27%) of simulated experiments yield a smaller LB (NN) maximum likelihood.

We bin data and the MC signal plus background events in the  $m_{\text{fit}}, D(\mathbf{x})$  array for each of the MC signal event sets in the  $m_t$  range from 150 to 200 GeV/ $c^2$ . In order to improve the accuracy of the  $m_t$  determination, we have generated more events and in smaller  $m_t$  steps in the region where we have subsequently seen MC and data to agree the best. For each of the MC sets we assign a likelihood  $L$  which assumes that all samples obey Poisson statistics. Bayesian integration [18] over possible true signal and background populations in each bin yields

$$L(m_t, n_s, n_b) = \prod_{i=1}^M \sum_{j=0}^{n_i} \binom{n_{si} + j}{j} \binom{n_{bi} + k}{k} p_s^j (1 + p_s)^{-n_{si} - j - 1} p_b^k (1 + p_b)^{-n_{bi} - k - 1},$$

where  $n_s$  ( $n_b$ ) is the expected number of signal (background) events in the data;  $n_i$ ,  $n_{si}$ , and  $n_{bi}$  are the actual number of data, MC signal, and MC background events in bin  $i$ ;  $k \equiv n_i - j$ ;  $p_{s,b} \equiv n_{s,b} / (M + \sum_i n_{si,bi})$ ; and  $M = 40$  (200) bins for the LB (NN) methods. Maximizing  $L$  for each  $m_t$  gives the best estimates of  $n_s^*(m_t)$  and  $n_b^*(m_t)$  for  $n_s$  and  $n_b$ . Fig. 9(c) displays  $\ln L(m_t, n_s^*(m_t), n_b^*(m_t))$  versus  $m_t$  for  $\ln L$  calculated using both LB and NN methods.

Given the  $\ln L$  versus  $m_t$  distribution we perform a parabolic fit to the lowest point and its eight nearest neighbors from which we determine  $m_t$  and its statistical error  $\sigma_m$ . Table 3 presents the fit results which include  $m_t$  and the number of signal and background events which constitute the statistical classification of the 77 events contained in the sample described in subsection 3.2.

The LB and NN results  $m_t^{\text{LB}}$  and  $m_t^{\text{NN}}$  are mutually consistent, nevertheless we include half of  $m_t^{\text{LB}} - m_t^{\text{NN}}$  in the systematic error. To obtain the final  $m_t$  result, shown in Table 3, we combine  $m_t^{\text{LB}}$  and  $m_t^{\text{NN}}$  allowing for their  $(88 \pm 4)\%$  correlation (determined by MC experiments). Figs. 9(a–b) show that this result represents the data well.

Extensive MC studies summarized in Table 3 using 10,000 simulated experiments composed of 77 top + background events, with  $m_t$ ,  $\langle n_s \rangle$ , and  $\langle n_b \rangle$  as listed, yield a mean result  $\langle m_t \rangle$ , a mean statistical error  $\langle \sigma_m \rangle$ , and a range  $\pm \delta m$  within which 68% of the results fall. Using the LB (NN) method, 6% (25%) of the simulated experiments produce a  $\sigma_m$  which is smaller than we obtain. For the full ensemble,  $\delta m$  is larger than  $\sigma_m$  from our data. However, for “accurate subsets” of the ensemble for which the average  $\sigma_m / m_t$  is the same as we observe,  $\delta m$  is close to  $\sigma_m$ .

Table 3: Results of fits to data and MC events. Fits to data yield values and errors  $\sigma(\text{stat})$  for  $m_t$ ,  $n_s$ , and  $n_b$  (described in the text). Systematic errors are combined in quadrature. The resulting  $m_t$  and its statistical error  $\sigma_m$  are the combined LB and NN values. Fits to MC use ensembles of 10,000 simulated experiments composed of top + background, with  $m_t$ ,  $\langle n_s \rangle$ , and  $\langle n_b \rangle$  as listed. They yield a mean result  $\langle m_t \rangle$ , a mean statistical error  $\langle \sigma_m \rangle$ , and a range  $\pm \delta m$  within which 68% of the results fall. Using the LB (NN) method, 6% (25%) of the simulated experiments produce a  $\sigma_m$  which is smaller than we obtain. For an “accurate subset” of the MC ensembles with mean  $\sigma_m/m_t$  that matches our value,  $\delta m$  is smaller.

<b>Fits to data</b>		---LB fit---		---NN fit---		
Quantity fit		value	$\sigma(\text{stat})$	value	$\sigma(\text{stat})$	
$m_t$ (GeV/c <sup>2</sup> )		174.0	$\pm 5.6$	171.3	$\pm 6.0$	
$n_s$		23.8	+8.3 -7.8	28.8	+8.4 -9.1	
$n_b$		53.2	+10.7 -9.3	48.2	+11.4 -8.7	
<b>Systematic error on <math>m_t</math></b>		energy scale $\pm 4.0$				
		generator $\pm 4.1$				
		other $\pm 2.2$				
<b>Resulting <math>m_t</math> (GeV/c<sup>2</sup>)</b>		<b>173.3 <math>\pm 5.6</math> (stat) <math>\pm 6.2</math> (syst)</b>				
<b>Fits to MC</b>	type	----input----			----output----	
(top + background)	of fit	$m_t$	$\langle n_s \rangle$	$\langle n_b \rangle$	$\langle \sigma_m \rangle$	$\langle m_t \rangle$ $\delta m$
full ensemble	LB	175	24	53	9.9	175.0 8.7
"	NN	172	29	48	8.5	171.6 8.0
accurate subset	LB	175	24	53	5.5	175.3 4.6
"	NN	172	29	48	5.8	172.0 6.0

### 3.5 Systematic Errors; $t\bar{t}$ Signal and Background Predictions

We use the HERWIG MC [9] to simulate top signal, and the VECBOS MC [13] (with HERWIG fragmentation of partons into jets) to simulate the distributions of the  $W$ +multijet background. The  $\approx 20\%$  of background events from non- $W$  sources are modeled by multijet data.

The systematic errors include an error due to the uncertainty in the jet energy scale

of  $\pm(2.5\% + 0.5 \text{ GeV})$  which was determined studying  $Z \rightarrow ee$  events,  $E_T$  balance in  $\gamma$ +jet events and the differences between the data and the MC. We estimate the uncertainties in modeling of QCD by substituting the ISAJET MC generator [12] for HERWIG, independently for top MC and for VECBOS fragmentation, and by changing the VECBOS QCD scale from jet  $\langle p_T \rangle^2$  to  $M_W^2$ . Other effects include noise, multiple  $p\bar{p}$  interactions, and differences in fits to  $\ln L$ . All systematic errors shown in Table 3 sum in quadrature to  $\pm 6.2 \text{ GeV}/c^2$ .

## 4 Summary

We have performed the measurement of the  $t\bar{t}$  production cross section based on  $ee$ ,  $e\mu$ ,  $\mu\mu$ ,  $e\nu$ ,  $e$ +jets,  $\mu$ +jets,  $e$ +jets/ $\mu$ , and  $\mu$ +jets/ $\mu$  channels and the measurement of the top quark mass in the lepton+jets channel.

The results are:  $m_t = 173.3 \pm 5.6 \text{ (stat)} \pm 6.2 \text{ (syst)} \text{ GeV}/c^2$  and the corresponding production cross section:  $\sigma_{t\bar{t}} = 5.5 \pm 1.4 \text{ (stat)} \pm 0.9 \text{ (syst)} \pm 0.6 \text{ (gen)} \text{ pb}$ , which are in good agreement with the SM predictions. The results are summarized in Table 3, Figs. 9 and 5.

## 5 Acknowledgments

We would like to thank the organizers for a very interesting and enjoyable conference.

We thank the staffs at Fermilab and collaborating institutions for their contributions to this work, and acknowledge support from the Department of Energy and National Science Foundation (U.S.A.), Commissariat à l’Energie Atomique (France), State Committee for Science and Technology and Ministry for Atomic Energy (Russia), CNPq (Brazil), Departments of Atomic Energy and Science and Education (India), Colciencias (Colombia), CONACyT (Mexico), Ministry of Education and KOSEF (Korea), CONICET and UBACyT (Argentina), and the A.P. Sloan Foundation.

## References

- [1] CDF Collaboration, F. Abe *et al.*, Phys. Rev. Lett. **74**, 2626 (1995).
- [2] DØ Collaboration, S. Abachi *et al.*, Phys. Rev. Lett. **74**, 2632 (1995).

- [3] DØ Collaboration, S. Abachi *et al.*, submitted to Phys. Rev. Lett. (1997); Fermilab-Pub-97/109-E; hep-ex/9704015.
- [4] DØ Collaboration, S. Abachi *et al.*, submitted to Phys. Rev. Lett. (1997); Fermilab-Pub-97/059-E; hep-ex/9703008.
- [5] DØ Collaboration, S. Abachi *et al.*, Nucl. Instrum. Methods **A338**, 185 (1994).
- [6] DØ Collaboration, S. Abachi *et al.*, Phys. Rev. D**52**, 4877 (1995).
- [7] N. Amos *et al.*, Proc. Intl. Conf. on Computing in High Energy Physics, Rio de Janeiro, Brazil, ed. R. Shellard, T. D. Nguyen. (World Scientific, Singapore, 1995).
- [8] V. Barger, J. Ohnemus and R. J. N. Phillips, Phys. Rev. D **48**, 3953 (1993).
- [9] G. Marchesini *et al.*, Comp. Phys. Comm. **67**, 465, (1992).
- [10] R. Brun and F. Carminati, CERN Program Library Long Writeup W5013, 1993 (unpublished).
- [11] E. Laenen, J. Smith, and W. van Neerven, Phys. Lett. **B321**, 254 (1994).
- [12] F. Paige and S. Protopopescu, BNL Report BNL38034, 1986 (unpublished), release 7.21.
- [13] F. A. Berends, H. Kuijf, B. Tausk, and W. T. Giele, Nucl. Phys. B**357**, 32 (1991).
- [14] E. Berger and H. Contopanagos, Phys. Lett. **B361**, 115 (1995) and Phys. Rev. D **54**, 3085 (1996).
- [15] S. Catani, M.L. Mangano, P. Nason, and L. Trentadue, Phys. Lett. **B378**, 329 (1996).
- [16] S. Snyder, Ph.D. thesis, State Univ. of New York, Stony Brook, 1995 (unpublished), [http://www-d0.fnal.gov/publications\\_talks/thesis/snyder/thesis-ps.html](http://www-d0.fnal.gov/publications_talks/thesis/snyder/thesis-ps.html).
- [17] E.K. Blum and L.K. Li, Neural Networks **4**, 511 (1991); D.W. Ruck *et al.*, IEEE Trans. Neural Networks **1**, 296 (1990); L. Lönnblad *et al.*, Comput. Phys. Commun. **81**, 185 (1994); DØ Collaboration, P.C. Bhat, in Proc. 10<sup>th</sup> Topical Workshop on  $p\bar{p}$  Collider Physics, FNAL, 308 (1995), Fermilab-Conf-95/211-E. We used JETNET 3.0.
- [18] P.C. Bhat, H.B. Prosper, and S. Snyder, Fermilab-Pub-96/397, submitted to Phys. Lett. B.